Applied Catalysis B: Environmental 129 (2013) 394–402

Contents lists available at SciVerse ScienceDirect

Applied Catalysis B: Environmental

journal homepage: www.elsevier.com/locate/apcatb

Efficient anchorage of highly dispersed and ultrafine palladium nanoparticles on the water-soluble phosphonate functionalized multiwall carbon nanotubes

Min Zheng, Pan Li, Gengtao Fu, Yu Chen*, Yiming Zhou, Yawen Tang, Tianhong Lu

Jiangsu Key Laboratory of New Power Batteries, Laboratory of Electrochemistry, College of Chemistry and Materials Science, Nanjing Normal University, 1# Wenyuan Road, Nanjing 210046, PR China

ARTICLE INFO

Article history:
Received 8 May 2012
Received in revised form 4 August 2012
Accepted 28 September 2012
Available online 9 October 2012

Keywords:
Carbon nanotubes
Noncovalent functionalization
Phosphonic acid groups
Solubilization
Formic acid electrooxidation

ABSTRACT

A facile noncovalent approach is proposed to graft phosphonate groups onto the surface of the multiwall carbon nanotubes (MWCNTs) by π–π stacking interaction between naphthalen-1-ylmethylphosphonic acid (NYPA) and MWCNTs. Noncovalently attachment of phosphonate groups on the MWCNTs surface is confirmed by Fourier transform infrared (FT-IR) spectroscopy, X-ray photoelectron spectroscopy (XPS), Raman spectroscopy, and zeta potential analysis. The water-soluble phosphonate functionalized MWCNTs are further deposited with Pd nanoparticles (Pd-NPs) as electrocatalyst for formic acid oxidation. The morphology and structure of Pd-MWCNTs nanocomposites are characterized by transmission electron microscopy (TEM), X-ray diffraction (XRD) and XPS measurements. It is observed that Pd-NPs are highly dispersed and effectively anchored on the side walls of the phosphonate functionalized MWCNTs. The Pd-MWCNTs nanocomposites exhibit better electrocatalytic activity and long-term stability for formic acid electrooxidation than the un-phosphonated counterpart.

1. Introduction

The unique one-dimensional geometric structure, high electric conductivity, large surface area, good chemical and thermal stability, and excellent mechanical properties of carbon nanotubes (CNTs) make these excellent candidates for basic scientific study of material science [1–16]. However, the insolubility and the bundling of CNTs in aqueous solution, originated from their inert graphitic nature, strong hydrophobicity and strong intertube van der Waals interactions [17], impede seriously their applications in a number of important areas, such as nanoscale electronics [17,18], quantum devices [19], sensors [18], reinforcement for materials [20], support for catalysts [21], energy storage [3], and so on. Over the past decades, enormous efforts have been devoted to addressing the insolubility problem. One of the most commonly used strategies to render CNTs soluble in aqueous media is through their surface functionalization to form the kinetically stable suspension [4,19].

Chemical modification of side walls, defect sites, and open ends has been used to impart solubility to CNTs. It is well known that the oxidatively shortened CNTs are inherently soluble in water owing to ionic defects at side walls and tube ends [22]. Tube ends and side walls of the oxidative CNTs can be further functionalized by water-solubilizing agents via covalent approach. Unfortunately, the covalent chemistry dramatically alters the atomic and electronic structures of CNTs, causing the loss of the electrical properties and the degradation of their mechanical strength and chemical stability [22]. Functionalization of the CNTs can also been achieved by noncovalent (supramolecular) approach, which generally retains the electronic structure of the CNTs. In the approach, the bundled nanotubes are individually dispersed via physical adsorption, using suitable solubilizers (such as surfactant or biological polymers) to overcome the hydrophobic interactions between CNTs by means of the electrostatic repulsion force between solubilizer molecules, and/or the hydrophilic property of solubilizer molecules [23]. Another strategy of CNTs solubilization is to anchor ionic charges on the CNTs surface via suitable linker groups. Herein, several aromatic organic compounds, such as derivatives of pyrene, porphyrin and phthalocyanine, can adsorb on the CNTs surface via π–π stacking. In a polar medium, the major contributions to π–π stacking result from electrostatic interactions, van der Waals interactions, and/or hydrophobic interactions between CNTs surface and aromatic compounds [20,22]. The straightforward preparation has also the advantage of maintaining the structure of the CNTs [23], similar to noncovalent (supramolecular) attachment method.

Phosphonates and organophosphates are structurally similar. The organophosphate has four oxygens with an alkyl group connected via a phosphoester bond, while the phosphonates have three oxygens with a carbon attached directly to phosphorus. The lack of the hydrolyzable C—O—P linkage makes the phosphonate compounds more stable in aqueous solution than the organophosphate compounds [24]. The phosphonic acid groups ($-PO_3H_2$) terminated functional interface has been applied in various fields such

* Corresponding author. Tel.: +86 25 85891651; fax: +86 25 83243286.
E-mail address: ndchenyu@yahoo.cn (Y. Chen).

0926-3373/$ – see front matter © 2012 Elsevier B.V. All rights reserved.
http://dx.doi.org/10.1016/j.apcatb.2012.09.047

as ZrP materials [25], gold surface modification [26,27], metal ion recognition [28], biomimetic membrane [29,30], electrochemical sensor [24,31–33] oriented nucleation of minerals [34], and enzyme immobilization [29,35–37], owing to its excellent biocompatibility, strong coordination ability and adjustable interfacial charge density, etc. Up to now, the carboxylated CNTs and the sulfonated CNTs have been extensively studied and used in various fields. Surprisingly, little attention has been given to the phosphonate functionalized CNTs. To the best of our knowledge, the phosphonate functionalized CNTs have thus far been reported in only two cases. In both cases, the phosphonate functionalized CNTs were synthesized by covalent functionalization method. Namely, the phosphonate functionalized CNTs were prepared by reacting fluorinated CNTs (CNTs-F) with the 3-aminopropyl-phosphonic acid [38], or by reacting the carboxylated CNTs (CNTs-COOH) with 2-aminoethyl phosphonic acid [39,40]. Since phosphonic acid ($-PO_3H_2$) group is a dibasic acid, the electrostatic repulsion between $-PO_3^{2-}$ species is expected to be much stronger than that between $-COO^-$ or $-SO^{3-}$ groups according to Coulomb's law [29]. Moreover, $-PO_3H_2$ groups are extremely hydrophilic [41]. Such a strong electrostatic repulsion together with the excellent hydrophilic property of the $-PO_3^{2-}$ groups should facilitate the solubility of the CNTs [29]. However, phosphonate functionalized CNTs prepared by Pillai are insoluble in water [40], which may be attributed to the low functionalization degree due to the limitation of covalent modification.

Palladium (Pd) is an important noble metal that is widely recognized in heterogeneous catalysis, electroanalysis and hydrogen storage [42–49]. In order to disperse Pd nanoparticles (Pd-NPs) and to improve their catalytic efficiency, the CNTs are generally used as supporting materials due to their fascinating structures and electrical/mechanical properties [50–52]. For synthesis of Pd/CNTs nanocomposites, it is necessary to functionalize the graphitic surfaces of the CNTs since the pristine surface of the CNTs is chemically inert and hydrophobic. The most commonly used method is to oxidize CNTs by various oxidizing agents to introduce hydrophilic O-containing groups on the CNTs surface [3], which can effectively anchor and deposit Pd-NPs. It is worth noting that the CNTs are not ideal structures, but rather contain defects formed during synthesis. Typically around 1–3% of the carbon atoms of a nanotube are located at a defect site [53]. A frequently encountered type of defect is the so-called Stone–Wales defect, which is comprised of two pairs of five-membered and seven-membered rings [19,51]. Moreover, the ends of the CNTs are composed of five-membered rings. The previous reports have indicated five-membered and seven-membered rings at CNTs are more reactive than fullerenes at side walls of the CNTs [19,54]. Thus, functionalization of the side walls comprising the regular graphene framework is more difficult to accomplish. Indeed, O-containing surface groups are typically concentrated around the ends and the defects of the CNTs rather than side walls of the CNTs during oxidation treatment of the CNTs. Consequently, metal or metal oxides NPs are selectively immobilized at the ends and the defects of the CNTs during the synthesis of NPs/CNTs nanocomposites [55,56].

Direct formic acid fuel cells (DFAFCs) have attracted more and more attention as a new generation of environment-friendly portable power source with high operating power density [57,58]. The success of DFAFCs largely depends on the design and the preparation of the high performance anode catalyst [58–66]. Recent investigations have suggested that Pd catalysts, an inexpensive non-Pt catalyst, possess far better electrocatalytic activity for formic acid oxidation than Pt catalysts. In the present work, the water-soluble phosphonate functionalized multiwall carbon nanotubes (MWCNTs) were for the first time synthesized by π–π stacking interaction between naphthalen-1-ylmethylphosphonic acid (NYPA, shown in Scheme 1A) and MWCNTs. The resulting phosphonate functionalized MWCNTs were further deposited with Pd-NPs as electrocatalyst for formic acid oxidation. Structural characterizations revealed that the well-dispersed Pd- NPs with an average size of 3 nm were loaded on the phosphonate functionalized MWCNTs surface. Electrochemical measurements displayed that the Pd-MWCNTs nanocomposites had the excellent electrocatalytic performance for formic acid oxidation.

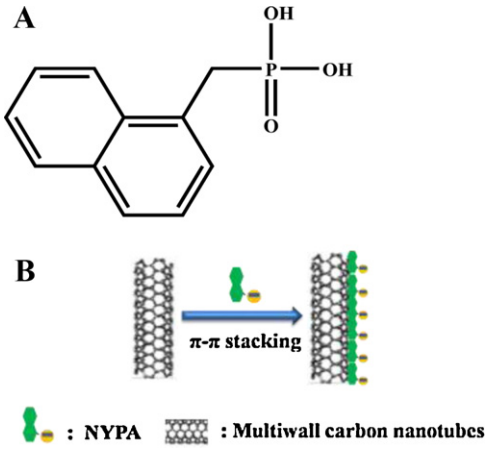

Scheme 1. (A) Structure of naphthalen-1-ylmethylphosphonic acid (NYPA); (B) Schematic noncovalent functionalization of MWCNTs with NYPA.

2. Experimental

2.1. Reagents and chemicals

Crude multiwall carbon nanotubes (MWCNTs) (>95% purity; outer diameter 35–60 nm; inner diameter 25–40 nm; length 5–10 μm; surface area: 180.6 $m^2 g^{-1}$) used in this study were purchased from Chengdu Organic Chemicals Co. Ltd., Chinese Academy of Sciences, which were prepared by a catalytic decomposition method of hydrocarbons. The synthetic naphthalen-1-ylmethylphosphonic acid (NYPA) was gifted by Dr. Pengfei Wang at Nanjing University. Palladium chloride ($PdCl_2$) was purchased from Sinopharm Chemical Reagent Co., Ltd. (Shanghai, China). All other reagents were of analytical grade and used without further purification. All the aqueous solutions were prepared with Millipore water having a resistivity of 18.2 MΩ.

2.2. Purification of the MWCNTs

Crude MWCNTs were purified by oxidation method [21]. Briefly, MWCNTs were pretreated carefully with concentrated HCl (12 M) for 2 h and concentrated HNO_3 (14 M) for 2 h at 50 °C, consecutively. After filtration and dryness, ICP analysis showed metal (Fe, Co, Ni and La) loadings of the MWCNTs was lower than 1.5 mg g^{-1}, indicating the metal particles contained in the MWCNTs as the synthesis catalyst during production were removed. Meanwhile, XPS measurement indicated the oxidation method resulted in the generation of the oxygenous functional groups on the MWCNTs surface (Fig. S1). Theoretically, the produced oxygenous functional groups affected the surface modification of MWCNTs via π–π stacking method due to the space hindrance effect. Thus, possible surface functional groups like —OH and —COOH on the pretreated MWCNTs surface were removed by heat treatment at 500 °C for 3 h in N_2 [22]. After the heat treatment, the reversible redox peaks of the oxidative MWCNTs [67] disappeared (Fig. S2), confirming the surface of MWCNTs had been cleaned successfully.

2.3. Modification of the MWCNTs

60 mg pre-treated MWCNTs were added to 60 mL of 5 mM NYPA aqueous solution (pH 9), and sonicated for 2 h in an ice water bath [68]. After sonication, the resultant suspension was centrifuged at 4000 rpm to remove insoluble amorphous carbon. Then, the supernatant solution was filtered with polycarbonate membrane, and washed several times with water. After drying at 60 °C for 10 h in a vacuum oven, the NYPA modified MWCNTs (i.e., NYPA-MWCNTs) were obtained.

2.4. Preparation of NYPA-MWCNTs supported Pd-NPs catalyst

In a typical procedure, 3.1 mL of 0.045 M $PdCl_2$ and 60 mg NYPA-MWCNTs were added into 10 mL water and sonicated for 30 min to achieve a homogeneous dispersion. After the pH value of the suspension solution was adjusted to 6.5, the suspension was heated at 70 °C for 3.5 h. Then, 20 mL 0.067 M $NaBH_4$ solution was added to the suspension and the resulting suspension was stirred for an additional 60 min. After filtration, wash and dryness, the NYPA-MWCNTs supported Pd-NPs catalyst (Pd/NYPA-MWCNTs) was obtained. For comparison, the un-modified MWCNTs were also been used to synthesize MWCNTs supported Pd-NPs catalyst (Pd/UN-MWCNTs) by the above preparation method.

2.5. Electrochemical measurements

Electrochemical measurements were performed by using a CHI 660C electrochemical analyzer (CH Instruments, Shanghai Chenghua Co.) in a conventional three-electrode electrochemical cell. A Pt plate auxiliary electrode and a saturated calomel reference electrode (SCE) were used. All potentials in this study were reported with respect to SCE. For the preparation of working electrode, the typical process followed the previous procedure reported [69]. An evenly distributed suspension of catalyst was prepared by sonicating the mixture of 4 mg catalyst and 1.6 mL H_2O for 30 min, and 4 μL the resulting suspension was laid on the surface of the pre-cleared glassy carbon electrode (3 mm diameter, 0.07 cm^2). After drying at room temperature, 3.0 μL of Nafion 5.0 wt% solutions were covered on the surface of the catalyst electrode and allowed to dry again. Thus, the working electrode was obtained, and the specific loading of Pd metal on the electrode surface was about 28 μg cm^{-2}. Prior to the electrochemical measurements, N_2 was bubbled through the solution for 10 min to remove the dissolved O_2. During experiments, a continuous N_2 flow was maintained over the solution. All the electrochemical measurements were carried out at 30 ± 1 °C.

2.6. Physical characterization

Surface area of the MWCNTs was measured by nitrogen adsorption at 77 K on a Micromeritics ASAP 2020 instrument. Raman spectra of carbon materials were examined with Labram HR 800 UV Raman spectrometer, equipped with a confocal microscope and an Ar ion laser (λ = 514.5 nm). High-resolution X-ray photoelectron spectroscopy (XPS) measurements were carried out on a Thermo VG Scientific ESCALAB 250 spectrometer with an Mg Kα radiator, and the vacuum in the analysis chamber was maintained at about 10^{-9} mbar or lower. Detailed Pd 3d and P 2p signals were collected and analyzed. The binding energy was calibrated by means of the C 1s peak energy of 284.6 eV. The curves were fitted by using the XPSPEAK41 software. Fourier transform infrared (FT-IR) spectra were carried out using a Nicolet 520 SXFTIR spectrometer. The spectra were collected in the wave number range between 400 and 4000 cm^{-1} over 128 scans at a resolution of 4 cm^{-1}. XRD measurements of catalysts were performed with Model D/max-rC diffractometer using Cu-Kα radiation (λ = 0.15406 nm) and operating at 45 kV and 100 mA. The morphology and particle size of catalysts were investigated using a JEOL JEM-2010 transmission electron microscope (TEM) operated at 200 kV accelerating potential. The metal loading in sample was accurately determined with a Leeman inductively coupled plasma atomic emission spectrometry (ICP-AES). The surface charge density of MWCNTs was characterized by zeta potential measurement using Malvern Zetasizer Nano ZS90. Dynamic light scattering (DLS) measurements were performed with Malvern Zetasizer Nano ZS90.

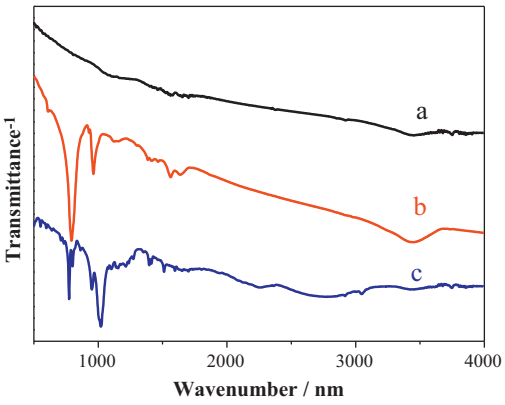

Fig. 1. FT-IR spectra of (a) un-modified MWCNTs, (b) NYPA-MWCNTs and (c) NYPA.

3. Results and discussion

3.1. Characteristics of the phosphonate functionalized MWCNTs

Noncovalent surface modification is an efficient and less-destructive approach to improve the solubility and the dispersibility of the CNTs through π–π stacking interaction, van der Waals interaction, and/or hydrophobic interaction between CNTs surface and either aromatic compounds [20]. In theory, the phosphonate functionalized MWCNTs can be easily obtained by sonicating the mixture solution of NYPA and MWCNTs, as shown in the Scheme 1B.

Fig. 1 shows FT-IR spectra of the MWCNTs before and after phosphonate functionalization, respectively. Un-modified MWCNTs have some weak peaks at 1570 cm^{-1} and 3420 cm^{-1} (Fig. 1a), which are attributed, respectively, to the C=C stretching of the MWCNTs [70] and the asymmetric bending arised from trace amounts of water [71]. After functionalization, NYPA-MWCNTs hybrids show a series of characteristic peaks of the phosphonic acid group in the range of 1300–400 cm^{-1} (Fig. 1b) [39,72]. All these absorption bands are similar to those of NYPA (Fig. 1c), indicating that NYPA molecules have successfully grafted on the MWCNTs surface.

XPS is a powerful tool for the investigation of CNTs-based hybrids due to its nature of surface-sensitive technique. The further evidence for the successful phosphonate modification of the MWCNTs was provided by the XPS spectra (Fig. S3). The appearance of the P2p peak (133.24 eV) confirms the successful immobilization of NYPA on the MWCNTs surface, which is not observed in the spectrum of un-modified MWCNTs. The surface morphologies of un-modified and functionalized MWCNTs were characterized by TEM images (Fig. S4). Compared to un-modified MWCNTs, the NYPA monolayer located outside of NYPA-MWCNTs hybrids is not visible in the low magnification TEM image due to the small molecule size of NYPA itself.

Raman spectra of un-modified MWCNTs and NYPA-MWCNTs hybrids are shown in Fig. 2. The un-modified MWCNTs exhibit two characteristic peaks at 1353.9 and 1582.6 cm^{-1}, corresponding to the D band (C—C, disordered graphite structure) and the G

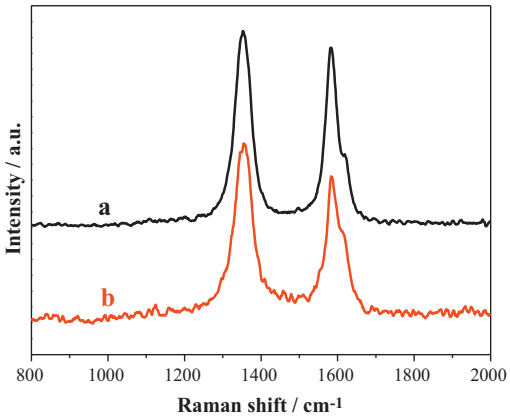

Fig. 2. Raman spectra of (a) un-modified MWCNTs and (b) NYPA-MWCNTs.

Fig. 3. Digital photographs of (a) 5 mg mL^{-1} un-modified MWCNTs and (b) 5 mg mL^{-1} NYPA-MWCNTs dispersed in water for 30 min.

band (C=C, tangential graphite mode), respectively. Such D and G bands are also strongly observed for the NYPA-MWCNTs. The intensity ratio of the D band to the G band of the CNTs, denoted as I_D/I_G, directly indicates the structural change of the CNTs after hybridization. The I_D/I_G ratios of the un-modified MWCNTs and NYPA-MWCNTs hybrids are 1.06 and 1.22, respectively. This result indicates the numbers of disordered carbons increase slightly after the functionalization of the MWCNTs [73–75], which is likely attributed to the introduction of CH_2 group in NYPA molecule and/or the damage of MWCNTs itself due to sonication treatment.

The surface charge of NYPA-MWCNTs was characterized by zeta potential measurement. The zeta potential of as-prepared NYPA-MWCNTs suspension is as low as -35 ± 5 mV at pH 7.0, suggesting that the naphthyl group of NYPA is attached to the MWCNTs surface via π–π stacking and/or hydrophobic interactions while phosphonic acid groups remain free on the chain end, as illustrated in Scheme 1B. Thus, the surface of NYPA-MWCNTs hybrids is endowed with hydrophilicity and polarity due to the attached phosphonic groups, which makes them have good dispersibility in water. The stability of colloidal particles is generally affected by their surface charge. As mentioned above, the electrostatic repulsion between $-PO_3^{2-}$ groups is much stronger than that between $-COO^-$ or $-SO^{3-}$ groups. And, $-PO_3^{2-}$ groups are extremely hydrophilic [41]. These particular properties of the phosphonate groups may facilitate the solubility of NYPA-MWCNTs hybrids [29]. As respected, as-prepared NYPA-MWCNTs hybrids are found to be soluble in water with good storage stability at ambient temperature (Fig. 3b). No precipitation or flocculation is observed even after three months (data not shown). For comparison, the dispersion of un-modified MWCNTs in water is difficult, even with the help of sonication. As can been seen in Fig. 3a, un-modified MWCNTs bear almost no dispersibility at all. Obviously, the excellent stability of NYPA-MWCNTs hybrids is attributed to above-mentioned electrostatic repulsion and hydration force of phosphonate groups. The colloidal stability of the NYPA-MWCNTs hybrids was further identified with the dynamic light scattering (DLS) measurement [73]. The statistical size distribution of NYPA-MWCNTs hybrids in water is shown in Fig. 4A. The average size of the NYPA-MWCNTs hybrids is approximately 215 nm. After three months of storage, the average size of NYPA-MWCNTs hybrids almost keeps constant (Fig. 4B). This result indicates NYPA-MWCNTs hybrids possess the excellent water-solubility, again.

3.2. Synthesis and characterization of NYPA-MWCNTs supported Pd-NPs catalyst

Pd/NYPA-MWCNTs catalyst was synthesized using the improved homogeneous precipitation–reduction reaction method reported previously by us [76], as illustrated in Scheme 2. Briefly, pH value of $PdCl_2$ solution was adjusted to 6.5, and the resulting $PdCl_2$ solution (pH 6.5) was heated slowly to generate $PdO{\cdot}H_2O$-NPs. Then, the formed $PdO{\cdot}H_2O$-NPs was reduced to obtain Pd^0-NPs by using $NaBH_4$ as reduction reagent.

The exact Pd loadings of catalysts were evaluated by ICP-AES analysis. All Pd/MWCNTs catalysts contain about 20.6 wt% Pd, nearly the same as the pre-set values. XPS measurements show atomic ratios of Pd^0/Pd^{II} in Pd/UN-MWCNTs and Pd/NYPA-MWCNTs catalysts are about 76:24 and 80:20, respectively (Fig. S5), which is higher than the reported values of Pd-NPs with similar particle size [77,78]. These results indicate that Pd^{II} precursor is successfully reduced to form metallic Pd in our synthesis. The

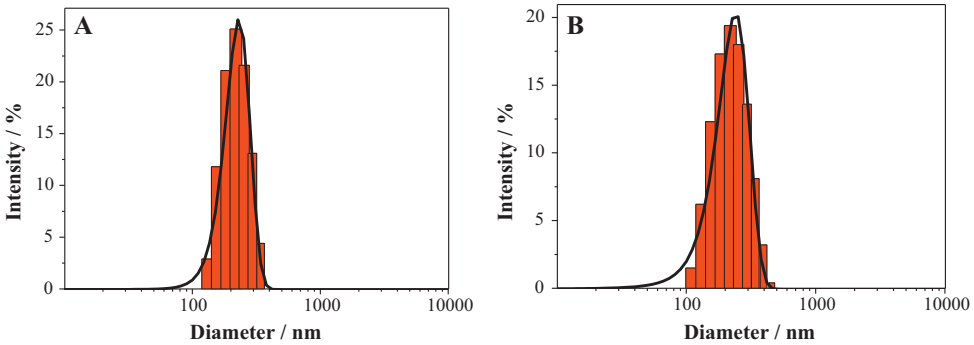

Fig. 4. DLS analysis of 0.2 mg mL^{-1} NYPA-MWCNTs aqueous suspension after (A) 30 min and (B) three months of storage.

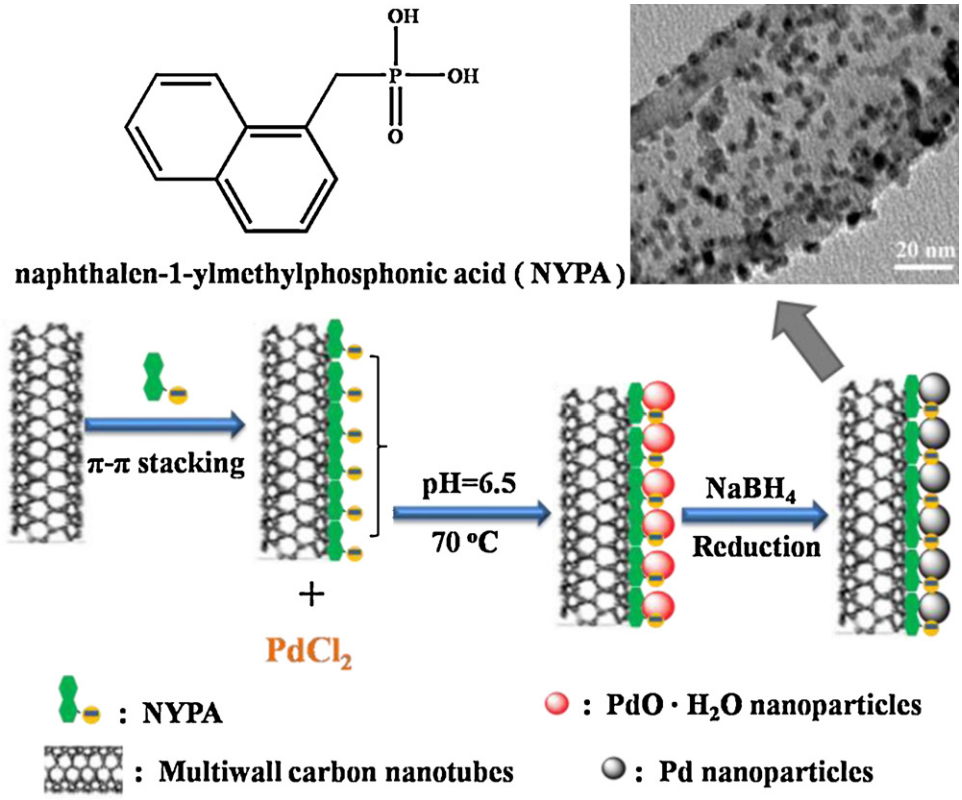

Scheme 2. Synthesis procedure of Pd/NYPA-MWCNTs catalyst.

crystalline nature of Pd-NPs on MWCNTs surface was confirmed by recording the XRD (Fig. 5). In each XRD pattern, it is observed that the diffraction peaks of Pd(1 1 1), Pd(2 0 0), Pd(2 2 0) and Pd(3 1 1) are located at 2θ values of 40.0°, 45.7°, 67.7° and 80.4°, respectively, illustrating that Pd-NPs possess the face centered cubic crystal structure. The average size of Pd-NPs can be calculated from the half peak width of the Pd(2 2 0) peak according to Scherrer equation [79]. The average sizes of Pd-NPs at Pd/UN-MWCNTs and Pd/NYPA-MWCNTs catalysts are cursorily calculated to be 3.3 and 2.7 nm, respectively.

Although the average size of Pd-NPs can be estimated according to XRD data, TEM characterization is more intuitive and reliable for this parameter. Fig. 6 shows typical TEM images and corresponding particle size distribution histogram of Pd/NYPA-MWCNTs catalyst. It is observed that spherical Pd-NPs are highly dispersed on the MWCNTs surface (Fig. 6A). According to distribution histogram, the average particle size of Pd-NPs at Pd/NYPA-MWCNTs catalyst is 2.9 nm with narrow size range between 1.7 and 5.0 nm (Fig. 6B). It is worth noting that as-prepared Pd/NYPA-MWCNTs catalyst still possesses the excellent dispersion and small particle size when Pd loading increases to 40 wt.% (Fig. S6). These TEM images indicate that the improved homogeneous precipitation–reduction reaction method used in this work is very efficient for the preparation of the high quality Pd/MWCNTs catalyst. As comparison, the dispersion of Pd-NPs at Pd/UN-MWCNTs catalyst is uneven with heavy agglomeration (Fig. S7). In addition, the heavy agglomeration of Pd-NPs is also observed when the carboxylated MWCNTs (MWCNTs-COOH) is used as carbon supporting material to synthesize Pd/MWCNTs-COOH catalyst (Fig. S8). Obviously, the high quality Pd/MWCNTs catalyst can be synthesized by using the phosphonate functionalized MWCNTs as carbon supporting material.

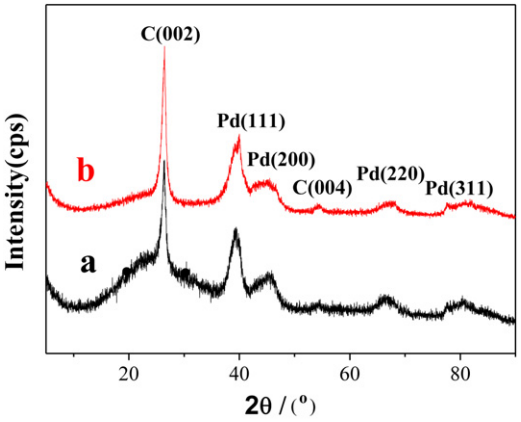

Fig. 5. XRD patterns of (a) Pd/UN-MWCNTs and (b) Pd/NYPA-MWCNTs.

3.3. Formation mechanism of highly qualitative Pd/NYPA-MWCNTs catalyst

For $PdCl_2$ aqueous solution, $[PdCl_4]^{2-}$ is the predominant species under the strong acidic conditions. With the increase of pH, the Cl^- ligand can be displaced by water molecule, and then neutral hydrated ion undergo hydrolysis and loss of proton. These processes can be represented by the following equation [80–83].

$$PdCl_4^{2-} + H_2O \leftrightarrow [PdCl_3(H_2O)]^- + Cl^- \quad (1)$$

$$[PdCl_3(H_2O)]^- \leftrightarrow [PdCl_3(OH)]^{2-} + H^+ \quad (2)$$

$$[PdCl_3(OH)]^{2-} + H_2O \leftrightarrow [PdCl_2(OH)(H_2O)]^- + Cl^- \quad (3)$$

$$[PdCl_2(OH)(H_2O)]^- \leftrightarrow [PdCl_2(OH)_2]^{2-} + H^+ \quad (4)$$

$$[PdCl_2(OH)_2]^{2-} + H_2O \leftrightarrow [PdCl(OH)_2(H_2O)]^- + Cl^- \quad (5)$$

$$[PdCl(OH)_2(H_2O)]^- \leftrightarrow [PdCl(OH)_3]^{2-} + H^+ \quad (6)$$

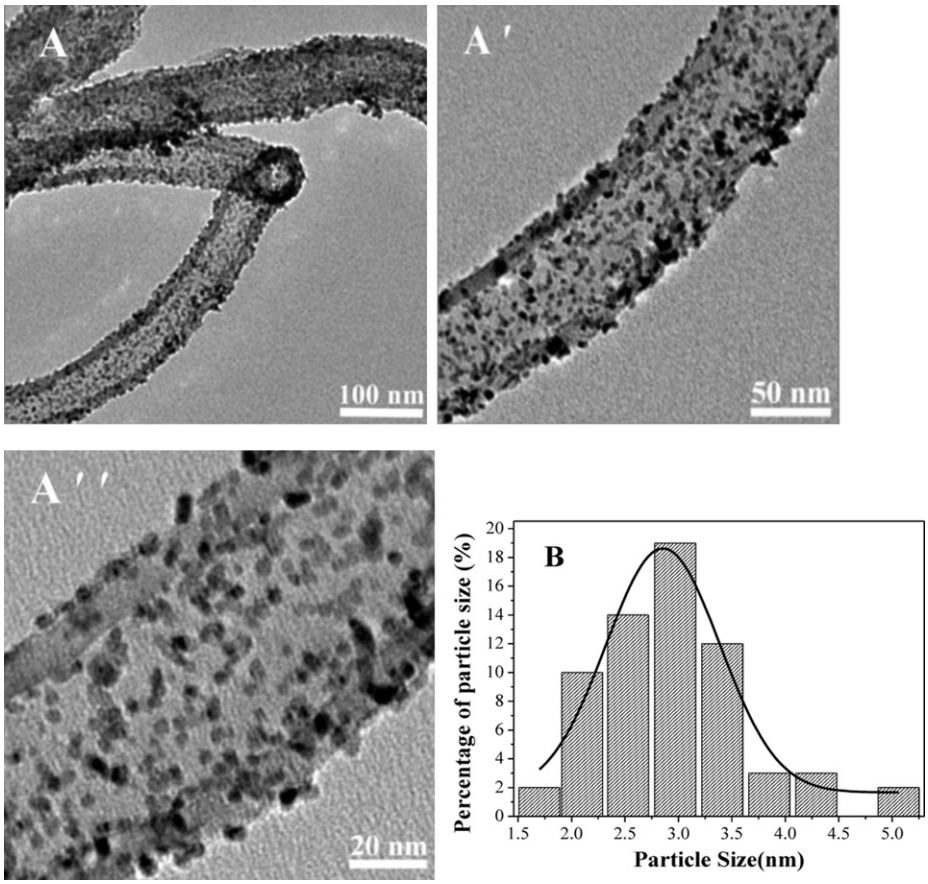

Fig. 6. (A, A′, A″) Typical TEM images and (B) corresponding size distribution histogram of Pd/NYPA-MWCNTs catalyst.

$$[PdCl(OH)_3]^{2-} + H_2O \leftrightarrow [Pd(OH)_3(H_2O)]^- + Cl^- \quad (7)$$

$$[Pd(OH)_3(H_2O)]^- \leftrightarrow [Pd(OH)_4]^{2-} + H^+ \quad (8)$$

The hydrolyzates of $[PdCl_4]^{2-}$ are extremely unstable even though under the weak basic condition because these hydrolyzates can easily transformed into highly insoluble palladium oxide hydrate ($PdO{\cdot}H_2O$) [84]. Since the hydrolysis of metal ion is generally an endothermic reaction, the hydrolysis of $PdCl_2$ is without exception, too. Our previous works have confirmed the hydrolyzates of $PdCl_2$ (pH 5.9) can slowly transformed into the red flocculent $PdO{\cdot}H_2O$ precipitate at 70 °C [84]. Similar to the case of homogeneous precipitation achieved by thermal decomposition of urea [85–87], the slow hydrolysis rate facilities the formation of $PdO{\cdot}H_2O$-NPs with uniform particle size because homogeneous precipitation method allows ripening of particles due to a slow reaction rate. In fact, our previous work [84] have found that the Vulcan XC-72 carbon supported Pd-NPs (Pd/C) catalyst prepared with homogeneous precipitation–reduction reaction method has better dispersion and smaller particle size compared to Pd/C catalyst prepared with the general $NaBH_4$ reduction method [42,88–91].

Since the homogeneous precipitation–reduction reaction method involves in $Pd^{II} \rightarrow PdO{\cdot}H_2O \rightarrow Pd^0$ reaction path, the particle size and dispersion of Pd-NPs at Pd/support catalyst depend on that of $PdO{\cdot}H_2O$-NPs. So far, the surface functionalization of CNTs has been recognized as the effective approach to improve dispersion of metal oxide NPs because these introduced surface groups generally have certain interaction with metal oxide NPs [3]. The most commonly used method is to oxidize CNTs by strong acids to introduce carboxyl groups. Unfortunately, the introduced carboxyl groups are typically concentrated around caps and defects of the CNTs rather than side walls of the CNTs [55], which results in uneven immobilization of $PdO{\cdot}H_2O$-NPs on carboxylated MWCNTs, and consequently results in heavy aggregation of Pd-NPs on carboxylated MWCNTs after $NaBH_4$ reduction, as shown in Fig. S8. It is well known that the $-PO_3H_2$ groups have a strong affinity to metal oxide through stable M—O—P bonds, such as ZrO_2, TiO_2 and $PdO{\cdot}H_2O$, etc. [84,92–95]. In the case of Pd/NYPA-MWCNTs catalyst, a great deal of uniform distributed phosphonate groups on the NYPA-MWCNTs surface can afford abundant nucleation sites to firmly adsorb $PdO{\cdot}H_2O$-NPs, which ultimately improves the dispersion of Pd-NPs after $NaBH_4$ reduction, as shown by TEM images in Fig. 6A.

3.4. Formic acid electrooxidation on Pd/MWCNTs catalysts

Fig. 7 shows the cyclic voltammograms of Pd/NYPA-MWCNTs and Pd/UN-MWCNTs catalysts in the 0.1 M $HClO_4$ solution at the rate of 50 mV s^{-1}. The typical voltammetric curves of Pd-NPs in acid media are observed at Pd/UN-MWCNTs and Pd/NYPA-MWCNTs catalysts. It is well known that the hydrogen atoms are essentially absorbed into the Pd lattice by a "dissolution adsorption mechanism" [42,96–104]. Mainly, H^+ ions first adsorb onto the Pd surface and are subsequently reduced to give adsorbed hydrogen (H_{ad}). The adsorbed hydrogen atoms finally diffuse into the bulk Pd such that they lie underneath the first few atomic layers of Pd atoms forming absorbed hydrogen (H_{ab}). Thus, the oxidation peaks at −185 mV and −53 mV in Fig. 7 are assigned to the oxidation of absorbed hydrogen and adsorbed hydrogen in the positive scan direction [42,101,102]. Consequently, the electrochemically active surface area (ECASA) of Pd-based catalysts cannot be precisely assessed by coulometry in the "hydrogen region" due to the interference

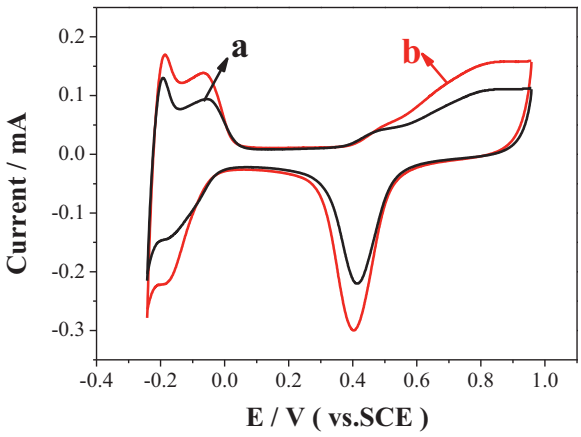

Fig. 7. Cyclic voltammograms of (a) Pd/UN-MWCNTs and (b) Pd/NYPA-MWCNTs catalysts in 0.1 M $HClO_4$ solution at the rate of 50 mV s^{-1}.

of hydrogen absorption in bulk Pd. Recently, it is reported that ECASA of Pd-based catalyst can be calculated from the integrated reduction charge of surface palladium oxide besides CO-stripping method [104,105]. For the palladium oxide method, +0.958 V is chosen as an upper limit in a solution of pH 1 to avoid the further oxidation of the Pd surface [104]. Thus, the characteristic reduction peaks in higher potential region (ca. 0.40 V) is attributed to reduction of $Pd(OH)_2$ on the Pd surface, which can reflect the number of Pd sites. According to the Coulomb law, charge amount associated with the reduction peak area of palladium oxide, the ECASA values of Pd/UN-MWCNTs and Pd/NYPA-MWCNTs are estimated to 94.6 and 144.4 $m^2\ g^{-1}$ Pd, respectively. The larger ECASA value of Pd/NYPA-MWCNTs catalyst is most likely due to the smaller size and the better dispersion of Pd-NPs on NYPA-MWCNTs surface, which is in accord with results of XRD and TEM described above.

Fig. 8A shows cyclic voltammograms of Pd/UN-MWCNTs and Pd/NYPA-MWCNTs catalysts in 0.5 M HCOOH + 0.5 M H_2SO_4 solution at the rate of 50 mV s^{-1}. In the positive scan direction, the main oxidation peaks of formic acid at Pd/UN-MWCNTs and Pd/NYPA-MWCNTs catalysts are located at 0.15 V and 0.05 V, respectively, which corresponds with the direct oxidation pathway of formic acid [106]. The lower oxidation peak potential suggests that Pd/NYPA-MWCNTs catalyst exhibits better electrocatalytic activity than Pd/UN-MWCNTs catalyst. In addition, the corresponding oxidation peak currents on Pd/UN-MWCNTs and Pd/NYPA-MWCNTs catalysts are 625 and 954.6 A g^{-1} Pd, respectively. It clearly demonstrated that the electrocatalytic mass activity of the Pd/NYPA-MWCNTs catalyst for the formic acid oxidation is about 1.5 times higher than Pd/UN-MWCNTs catalyst. To further evaluate the activity and stability of catalysts, chronoamperometry tests were conducted in 0.5 M H_2SO_4 + 0.5 M HCOOH solution at 0.1 V for 3000 s (Fig. 8B). It is observed that the formic acid oxidation currents at the Pd/UN-MWCNTs and Pd/NYPA-MWCNTs catalysts at 3000 s are 32.4 and 77.4 A g^{-1} Pd, corresponding to 6.3% and 15.0% of their initial values (taken at 20 s to avoid the contribution of the double-layer discharge and hydrogen adsorption [21,107]), respectively, confirming that the electrocatalytic activity and the stability of Pd/NYPA-MWCNTs catalyst are much better than that of Pd/UN-MWCNTs catalyst. The previous XPS measurements indicate the binding energy of Pd-NPs at Pd/UN-MWCNTs and Pd/NYPA-MWCNTs is identical (Fig. S5). Thus, the electronic effect originated from the change of electronic structure of Pd atom is ruled out. Owing to the same loadings of Pd on the carbon supports, the enhanced electrocatalytic activity of Pd/NYPA-MWCNTs catalyst compared to Pd/UN-MWCNTs catalyst can be attributed to the small particle size and the excellent dispersion of Pd-NPs on NYPA-MWCNTs surface [44].

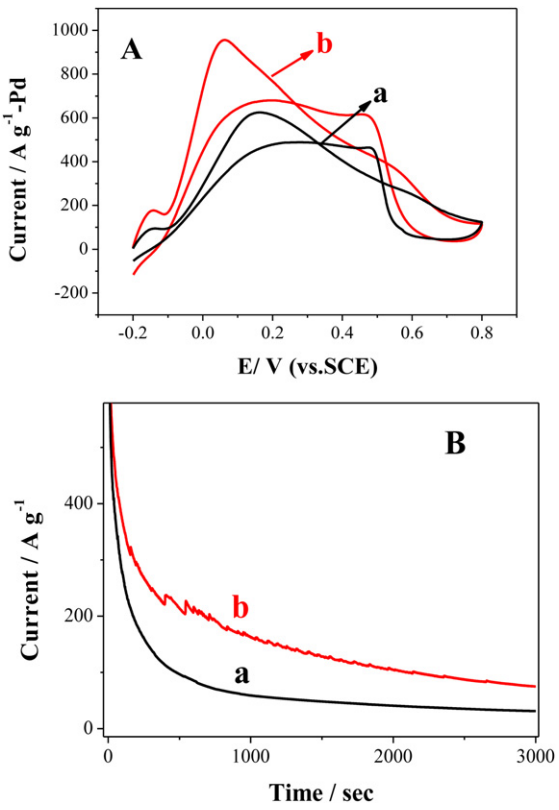

Fig. 8. (A) Cyclic voltammograms and (B) chronoamperometric curves of (a) Pd/UN-MWCNTs and (b) Pd/NYPA-MWCNTs catalysts in 0.5 M HCOOH + 0.5 M H_2SO_4 solution.

4. Conclusions

In this work, the phosphonate functionalized MWCNTs were for the first time synthesized by π–π stacking interaction between NYPA and MWCNTs. Introduction of the phosphonate groups into MWCNTs endowed MWCNTs unique properties, such as the high solubility in polar solvents and the excellent colloidal stability. The Pd/NYPA-MWCNTs nanocomposites with the excellent dispersion and the small particle size were easily synthesized by using improved homogeneous precipitation–reduction reaction method, which benefited from the strong interaction between $PdO{\cdot}H_2O$-NPs and the phosphonate groups on the NYPA-MWCNTs. Such Pd/NYPA-MWCNTs nanocomposites exhibited big electroactive surface area and high electrocatalytic activity toward formic acid oxidation. These results suggested that Pd/NYPA-MWCNTs nanocomposites developed in this study were a good candidate for heterogeneous catalyst or fuel cell electrode material.

Acknowledgments

The authors are grateful for the financial support of NSFC (21073094, 21273116 and 21005039), the United Fund of NSFC and Yunnan Province (U1137602), Natural Science Foundation of Jiangsu Higher Education Institutions of China (10KJB150007), Industry-Academia Cooperation Innovation Fund Project of Jiangsu Province (BY2012001), University Postgraduate Research and Innovation Project in Jiangsu Province (CX10S_036Z), and a project funded by the Priority Academic Program Development of Jiangsu Higher Education Institutions.

Appendix A. Supplementary data

Supplementary data associated with this article can be found, in the online version, at http://dx.doi.org/10.1016/j.apcatb.2012.09.047.

References

[1] A.D. Taylor, R.C. Sekol, J.M. Kizuka, S. DCunha, C.M. Comisar, Journal of Catalysis 259 (2008) 5–16.
[2] J. Chen, C.P. Collier, Journal of Physical Chemistry B 109 (2005) 7605–7609.
[3] W.D. Zhang, B. Xu, L.C. Jiang, Journal of Materials Chemistry 20 (2010) 6383–6391.
[4] A.H. Brozena, J. Moskowitz, B. Shao, S. Deng, H. Liao, K.J. Gaskell, Y.H. Wang, Journal of the American Chemical Society 132 (2010) 3932–3938.
[5] Y. Lu, J. Chen, Y. Liu, Q. Xue, M. He, Journal of Catalysis 254 (2008) 39–48.
[6] X. Yang, J. Zheng, M. Zhen, X. Meng, F. Jiang, T. Wang, C. Shu, L. Jiang, C. Wang, Applied Catalysis B: Environmental 121–122 (2012) 57–64.
[7] D. Wilson, W. Wang, R.J.G. Lopes, Applied Catalysis B: Environmental 123–124 (2012) 273–281.
[8] S. Takenaka, T. Arike, H. Matsune, M. Kishida, Applied Catalysis B: Environmental 125 (2012) 358–366.
[9] E.O. Jardim, M. Gonçalves, S. Rico-Frances, A. Sepulveda-Escribano, J. Silvestre-Albero, Applied Catalysis B: Environmental 113–114 (2012) 72–78.
[10] J. Chen, G. Li, Y. Huang, H. Zhang, H. Zhao, T. An, Applied Catalysis B: Environmental 123–124 (2012) 69–77.
[11] S. Zhang, Y. Shao, G. Yin, Y. Lin, Applied Catalysis B: Environmental 102 (2011) 372–377.
[12] R.P. Rocha, J.P.S. Sousa, A.M.T. Silva, M.F.R. Pereira, J.L. Figueiredo, Applied Catalysis B: Environmental 104 (2011) 330–336.
[13] A. Orfanidi, M.K. Daletou, S.G. Neophytides, Applied Catalysis B: Environmental 106 (2011) 379–389.
[14] S. Murugesan, K. Myers, V. Subramanian, Applied Catalysis B: Environmental 103 (2011) 266–274.
[15] Z. Li, B. Gao, G.Z. Chen, R. Mokaya, S. Sotiropoulos, G. Li Puma, Applied Catalysis B: Environmental 110 (2011) 50–57.
[16] Y.M. Dai, T.C. Pan, W.J. Liu, J.M. Jehng, Applied Catalysis B: Environmental 103 (2011) 221–225.
[17] C. Doe, S.M. Choi, S.R. Kline, H.S. Jang, T.H. Kim, Advanced Functional Materials 18 (2008) 2685–2691.
[18] Y. Wu, Food Chemistry 121 (2010) 580–584.
[19] I. Capek, Advances in Colloid and Interface Science 150 (2009) 63–89.
[20] M. Yu, S.Z. Zu, Y. Chen, Y.P. Liu, B.H. Han, Y. Liu, Chemistry: A European Journal 16 (2010) 1168–1174.
[21] Y. Chen, G. Zhang, J. Ma, Y. Zhou, Y. Tang, T. Lu, International Journal of Hydrogen Energy 35 (2010) 10109–10117.
[22] H. Paloniemi, T. Ritalo, T. Laiho, H. Liuke, N. Kocharova, K. Haapakka, F. Terzi, R. Seeber, J. Lukkari, Journal of Physical Chemistry B 109 (2005) 8634–8642.
[23] M. Fagnoni, A. Profumo, D. Merli, D. Dondi, P. Mustarelli, E. Quartarone, Advanced Materials 21 (2009) 1761–1765.
[24] Y. Chen, L.R. Guo, W. Chen, X.J. Yang, B. Jin, L.M. Zheng, X.H. Xia, Bioelectrochemistry 75 (2009) 26–31.
[25] X. Wang, M. Lieberman, Langmuir 19 (2003) 7346–7353.
[26] F. Zhang, Y. Zhou, Y. Chen, Z. Shi, Y. Tang, T. Lu, Journal of Colloid and Interface Science 351 (2010) 421–426.
[27] G.H. Woehrle, L.O. Brown, J.E. Hutchison, Journal of the American Chemical Society 127 (2005) 2172–2183.
[28] R.M. Petoral Jr., F. Bj refors, K. Uvdal, Journal of Physical Chemistry B 110 (2006) 23410–23416.
[29] Y. Chen, X.J. Yang, B. Jin, L.R. Guo, L.M. Zheng, X.H. Xia, Journal of Physical Chemistry C 113 (2009) 4515–4521.
[30] M.Y. Tsai, J.C. Lin, Journal of Biomedical Materials Research 55 (2001) 554–565.
[31] M. Zheng, Y. Zhou, Y. Chen, Y. Tang, T. Lu, Electrochimica Acta 55 (2010) 4789–4798.
[32] M. Zheng, Y. Chen, Y. Zhou, Y. Tang, T. Lu, Talanta 81 (2010) 1076–1080.
[33] Y. Chen, F.B. Wang, L.R. Guo, L.M. Zheng, X.H. Xia, Journal of Physical Chemistry C 113 (2009) 3746–3750.
[34] J. Aizenberg, J. Andrew, G.M. Whitesides, Journal of the American Chemical Society 121 (1999) 4500–4509.
[35] Y. Chen, B. Jin, L.R. Guo, X.J. Yang, W. Chen, G. Gu, L.M. Zheng, X.H. Xia, Chemistry: A European Journal 14 (2008) 10727–10734.
[36] Y. Chen, X.J. Yang, L.R. Guo, B. Jin, X.H. Xia, L.M. Zheng, Talanta 78 (2009) 248–252.
[37] Y. Chen, X.J. Yang, L.R. Guo, J. Li, X.H. Xia, L.M. Zheng, Analytica Chimica Acta 644 (2009) 83–89.
[38] A. Oki, L. Adams, V. Khabashesku, Y. Edigin, P. Biney, Z. Luo, Materials Letters 62 (2008) 918–922.
[39] T. Sainsbury, D. Fitzmaurice, Chemistry of Materials 16 (2004) 3780–3790.
[40] R. Kannan, P.P. Aher, T. Palaniselvam, S. Kurungot, U.K. Kharul, V.K. Pillai, The Journal of Physical Chemistry Letters 1 (2010) 2109–2113.
[41] H. Aoki, K. Hasegawa, K. Tohda, Y. Umezawa, Biosensors and Bioelectronics 18 (2003) 261–267.
[42] J.Y. Wang, Y.Y. Kang, H. Yang, W.B. Cai, Journal of Physical Chemistry C 113 (2009) 8366–8372.
[43] M. Sim es, S. Baranton, C. Coutanceau, Applied Catalysis B: Environmental 93 (2010) 354–362.
[44] C. Hu, Z. Bai, L. Yang, J. Lv, K. Wang, Y. Guo, Y. Cao, Electrochimica Acta 55 (2010) 6036–6041.
[45] L. Yuan, M. Yang, F. Qu, G. Shen, R. Yu, Electrochimica Acta 53 (2008) 3559–3565.
[46] G. Blanco-Brieva, M.P. de Frutos Escrig, J.M. Campos-Martin, J.L.G. Fierro, Green Chemistry 12 (2010) 1163–1166.
[47] V.R. Choudhary, C. Samanta, P. Jana, Industrial and Engineering Chemistry Research 46 (2007) 3237–3242.
[48] S. Park, S.H. Baeck, T.J. Kim, Y.M. Chung, S.H. Oh, I.K. Song, Journal of Molecular Catalysis A: Chemical 319 (2010) 98–107.
[49] G. Zhang, Y. Wang, X. Wang, Y. Chen, Y. Zhou, Y. Tang, L. Lu, J. Bao, T. Lu, Applied Catalysis B: Environmental 102 (2011) 614–619.
[50] S. Takenaka, N. Susuki, H. Miyamoto, E. Tanabe, H. Matsune, M. Kishida, Journal of Catalysis 279 (2011) 381–388.
[51] K. Balasubramanian, M. Burghard, Small 1 (2005) 180–192.
[52] W. Wang, Q. Huang, J. Liu, Z. Zou, M. Zhao, W. Vogel, H. Yang, Journal of Catalysis 266 (2009) 156–163.
[53] H. Hu, P. Bhowmik, B. Zhao, M. Hamon, M. Itkis, R. Haddon, Chemical Physics Letters 345 (2001) 25–28.
[54] E.V. Basiuk, M. Monroy-Pelcez, I. Puente-Lee, V.A. Basiuk, Nano Letters 4 (2004) 863–866.
[55] D. Eder, Chemical Reviews 110 (2010) 1348–1385.
[56] X. Li, J. Niu, J. Zhang, H. Li, Z. Liu, Journal of Physical Chemistry B 107 (2003) 2453–2458.
[57] S. Mahima, R. Kannan, I. Komath, M. Aslam, V.K. Pillai, Chemistry of Materials 20 (2007) 601–603.
[58] A. Miura, H. Wang, B.M. Leonard, H.D. Abruna, F.J. DiSalvo, Chemistry of Materials 21 (2009) 2661–2667.
[59] M. Ren, Y. Kang, W. He, Z. Zou, X. Xue, D.L. Akins, H. Yang, S. Feng, Applied Catalysis B: Environmental 104 (2011) 49–53.
[60] D. Tu, B. Wu, B. Wang, C. Deng, Y. Gao, Applied Catalysis B: Environmental 103 (2011) 163–168.
[61] B. Fang, M. Kim, J.S. Yu, Applied Catalysis B: Environmental 84 (2008) 100–105.
[62] S. Zhang, Y. Shao, H. Liao, J. Liu, I.A. Aksay, G. Yin, Y. Lin, Chemistry of Materials 23 (2011) 1079–1081.
[63] B.M. Leonard, Q. Zhou, D. Wu, F.J. DiSalvo, Chemistry of Materials 23 (2011) 1136–1146.
[64] V. Selvaraj, M. Alagar, K.S. Kumar, Applied Catalysis B: Environmental 75 (2007) 129–138.
[65] V. Selvaraj, M. Alagar, I. Hamerton, Applied Catalysis B: Environmental 73 (2007) 172–179.
[66] H. Meng, S. Sun, J.P. Masse, J.P. Dodelet, Chemistry of Materials 20 (2008) 6998–7002.
[67] C. Hu, W. Wang, K. Liao, G. Liu, Y. Wang, Journal of Physics and Chemistry of Solids 65 (2004) 1731–1736.
[68] B.X. Shi, Y. Wang, K. Zhang, T.L. Lam, H.L.W. Chan, Biosensors and Bioelectronics 26 (2010) 2917–2921.
[69] Y. Liang, Y. Zhou, J. Ma, J. Zhao, Y. Chen, Y. Tang, T. Lu, Applied Catalysis B: Environmental 103 (2011) 388–396.
[70] Y. Zhang, W. Cao, M. Liu, S. Yang, H. Wu, H. Lu, P. Yang, Molecular BioSystems 6 (2010) 1447–1449.
[71] B.D. Adams, G. Wu, S. Nigro, A. Chen, Journal of the American Chemical Society 131 (2009) 6930–6931.
[72] J.H. Yuan, Y. Chen, H.X. Zha, L.J. Song, C.Y. Li, J.Q. Li, X.H. Xia, Colloids and Surfaces B 76 (2010) 145–150.
[73] Q. Yang, X.J. Pan, Industrial & Engineering Chemistry Research 49 (2010) 2747–2751.
[74] L. Zhang, V.U. Kiny, H. Peng, J. Zhu, R.F.M. Lobo, J.L. Margrave, V.N. Khabashesku, Chemistry of Materials 16 (2004) 2055–2061.
[75] C.M. Chang, Y.L. Liu, Carbon 48 (2010) 1289–1297.
[76] J. Ma, Y. Ji, H. Sun, Y. Chen, Y. Tang, T. Lu, J. Zheng, Applied Surface Science 257 (2011) 10483–10488.
[77] L. Chen, A. Yelon, E. Sacher, Journal of Physical Chemistry C 115 (2011) 7896–7905.
[78] R. Wojcieszak, M. Genet, P. Eloy, P. Ruiz, E. Gaigneaux, Journal of Physical Chemistry C 114 (2010) 16677–16684.
[79] J. Xu, T. Zhao, Z. Liang, Journal of Power Sources 185 (2008) 857–861.
[80] L.I. Elding, L.F. Olsson, Journal of Physical Chemistry 82 (1978) 69–74.
[81] Q. Shen, Q. Min, J. Shi, L. Jiang, J.R. Zhang, W. Hou, J.J. Zhu, Journal of Physical Chemistry C 113 (2009) 1267–1273.
[82] Y. Shen, Q. Xu, H. Gao, N.N. Zhu, Electrochemistry Communications 11 (2009) 1329–1332.
[83] J.M. van Middlesworth, S.A. Wood, Geochimica et Cosmochimica Acta 63 (1999) 1751–1765.
[84] Y. Liang, M. Zhu, J. Ma, Y. Tang, Y. Chen, T. Lu, Electrochimica Acta 56 (2011) 4696–4702.
[85] L. Wang, I. Sondi, E. Matijevic, Journal of Colloid and Interface Science 218 (1999) 545–553.
[86] P.L. Chen, I. Chen, Journal of the American Ceramic Society 76 (1993) 1577–1583.

[87] M. Ogawa, H. Kaiho, Langmuir 18 (2002) 4240–4242.
[88] N. Hammer, S. Zarubova, I. Kvande, M. Ronning, Gold Bulletin 40 (2007) 234–239.
[89] H. Li, G. Sun, Q. Jiang, M. Zhu, S. Sun, Q. Xin, Journal of Power Sources 172 (2007) 641–649.
[90] M.R. Regan, I.A. Banerjee, Scripta Materialia 54 (2006) 909–914.
[91] W. Zhou, J.Y. Lee, Journal of Physical Chemistry C 112 (2008) 3789–3793.
[92] I. Doron-Mor, H. Cohen, S.R. Cohen, R. Popovitz-Biro, A. Shanzer, A. Vaskevich, I. Rubinstein, Langmuir 20 (2004) 10727–10733.
[93] Y. Chen, L.R. Guo, X. Kang, X.G. Liu, L.M. Zheng, X.H. Xia, Chinese Journal of Inorganic Chemistry 24 (2008) 2065–2070.
[94] S. zkar, R.G. Finke, Journal of the American Chemical Society 124 (2002) 5796–5810.
[95] S. Pawsey, M. McCormick, S. De Paul, R. Graf, Y. Lee, L. Reven, H.W. Spiess, Journal of the American Chemical Society 125 (2003) 4174–4184.
[96] G. Andreasen, A. Visintin, R. Salvarezza, W. Triaca, A. Arvia, Langmuir 15 (1999) 1–5.
[97] C. Batchelor-McAuley, C.E. Banks, A.O. Simm, T.G.J. Jones, R.G. Compton, ChemPhysChem 7 (2006) 1081–1085.
[98] M. Breiter, Journal of Electroanalytical Chemistry and Interfacial Electrochemistry 81 (1977) 275–284.
[99] M. Breiter, Journal of Electroanalytical Chemistry 109 (1980) 253–260.
[100] J. Horkans, Journal of Electroanalytical Chemistry 106 (1980) 245–249.
[101] H.P. Liang, N.S. Lawrence, T.G.J. Jones, C.E. Banks, C. Ducati, Journal of the American Chemical Society 129 (2007) 6068–6069.
[102] R. Pattabiraman, Applied Catalysis A: General 153 (1997) 9–20.
[103] X.M. Wang, Y.Y. Xia, Electrochimica Acta 54 (2009) 7525–7530.
[104] L. Xiao, L. Zhuang, Y. Liu, J. Lu, Journal of the American Chemical Society 131 (2008) 602–608.
[105] Y.W. Lee, M. Kim, S.W. Han, Chemical Communications 46 (2010) 1535–1537.
[106] R. Larsen, S. Ha, J. Zakzeski, R.I. Masel, Journal of Power Sources 157 (2006) 78–84.
[107] Y. Chen, Y. Zhou, Y. Tang, T. Lu, Journal of Power Sources 195 (2010) 4129–4134.